Electronic Supplementary Material (ESI) for Chemical Communications.

New structural approach to rationalize the foam film stability of oppositely charged polyelectrolyte/surfactant mixtures

Martin Uhlig,[ab] Oliver Löhmann,[c#] Salomé Vargas Ruiz,[a] Imre Varga,[d] Regine von Klitzing[ac*] and Richard A. Campbell[ef*]

a. Stranski-Laboratorium, Technische Universität Berlin, Berlin, Germany
b. Fraunhofer Center for Applied Nanotechnology (CAN), Hamburg, Germany
c. Physics Department, Technische Universität Darmstadt, Darmstadt, Germany
d. Institute of Chemistry, Eötvös Loránd University, Budapest, Hungary
e. Institut Laue-Langevin, 71 avenue des Martyrs, Grenoble, France
f. Division of Pharmacy and Optometry, University of Manchester, Manchester, UK
current address: European Spallation Source ESS ERIC, P. O. Box 176, Lund, Sweden

** corresponding authors: klitzing@fkp.tu-darmstadt.de and richard.campbell@manchester.ac.uk.*

Electronic Supplementary Information

1 Zeta Potential and UV-Visible Spectroscopy Data

The reason to choose a rather low value of [S], at only 3% of the critical micelle concentration, was to avoid pronounced time-dependent effects of precipitation in the P/S mixtures that can occur in more concentrated samples [1]. An indication of such effects is when polyelectrolyte/surfactant complexes (individual polyelectrolyte chains wrapping surfactant aggregates) are produced with a composition close to 1:1 stoichiometric charge binding, and the resulting lack of surface charge – and therefore lack of colloidal stability – leads to the formation of polyelectrolyte/surfactant aggregates (particles containing many polyelectrolyte chains wrapping surfactant aggregates). These liquid crystalline particles can reach the air/water interface under a variety of mechanisms [2] and then spread material to form kinetically-trapped films [3], which is a process that is affected by a variety of factors including the sample age and mixing protocols [4]. All samples were used within a few hours of mixing the components using a standard mixing approach [5], and they remained optically transparent to the eye throughout their use.

A bulk characterization of the samples was still carried out. The zeta potential measurements shown in Fig. SI1 demonstrate that the $sPSO_2$-220/C_{14}TAB complexes are negatively charged at all of the bulk compositions studied in the present work, and the values tends to even more negative values with increasing [P]. Nevertheless, in the samples with the lowest [P] measured, the zeta potential values approach zero, which indicate that the complexes formed may lack colloidal stability. The optical density of the samples recorded with a wavelength of 400 nm remains low, but the values increase slightly at high [P]. An extrapolation of a slope fitted to the last 4 data points of the optical density (when the zeta potential is strongly negative) to the samples with the lowest [P] indicate that the measured values of the optical density are slightly higher than could be expected. It may be the case therefore that in these samples a small number of aggregates is produced in the bulk upon mixing the components. However, due to the low bulk concentrations of the components, precipitation would be expected to be extremely slow, so influence of such a process can be excluded in the present work.

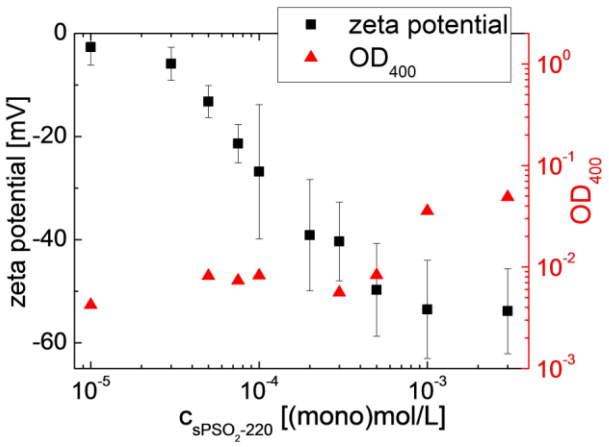

Fig. SI1. Values of the zeta potential and optical density at 400 nm (OD_{400}) of $sPSO_2$-220/$C_{14}TAB$ mixtures where [$C_{14}TAB$] = 10^{-4} M. The error bars for the zeta potential values correspond to the intrinsic experimental error of the instrument.

2 Further Experimental Details

2.1 Materials and sample preparation

Tetradecyltrimethylammonium bromide ($C_{14}TAB$) was purchased from Sigma-Aldrich (Steinheim, Germany) and recrystallized three times in acetone with traces of ethanol. To assess the purity of the surfactant surface tension measurements were performed. Chain-deuterated d_{29}-$C_{14}TAB$ ($dC_{14}TAB$) was purchased from CDN Isotopes (Quebec, Canada) and was used as received. D_2O was purchased from Sigma-Aldrich and was used as received. Monosulfonated poly(phenylene sulfone) ($sPSO_2$-220) was synthesized according to the guidelines in the literature [6]. It had a molecular mass of 100,000 g/mol and Li^+ as the counterion. To remove small ion impurities from synthesis, the $sPSO_2$-220 sample was diluted, with the resulting solution pressed through a syringe filter of 0.2 µm and then centrifuged at 4000 rpm for 60 min. The supernatant was collected and again centrifuged (with 1500 rpm and for 15 min) against centrifugal filters (Amicon Ultra 10K, Merck Millipore, Germany). The resulting supernatant of $sPSO_2$-220 was afterwards freeze dried and then re-diluted for experiments. Solutions were prepared by mixing equal volumes of $sPSO_2$-220/$C_{14}TAB$ stock solutions at twice the desired concentrations to limit the production of kinetically-trapped aggregates. All of the measurements were performed at 23–25 °C.

2.2 Zeta potential

The zeta potential was measured using a Malvern Zetasizer NanoZ (Malvern Instruments, Germany) instrument. The electrophoretic mobility was measured by performing Laser Doppler Electrophoresis. The zeta potential was then calculated by applying the Henry equation.

2.3 UV-visible spectroscopy

The turbidity of $sPSO_2$-220/$C_{14}TAB$ solutions was measured using a Varian Cary 50 UV–vis spectrophotometer. The optical density of the samples was determined at 400 nm (OD_{400}). Measurements were carried out 5 min after mixing. Since neither $sPSO_2$-220 nor $C_{14}TAB$ has an adsorption band above 350 nm, increasing OD_{400} values would indicate the presence of larger $sPSO_2$-220/$C_{14}TAB$ aggregates.

2.4 Surface tensiometry

The surface tension data of $sPSO_2$-220/C_{14}TAB mixtures in Fig. 1 of the main text are reproduced from ref. [7]. Values of the surface tension γ were measured using a K11 tensiometer (Krüss, Germany) with a du Noüy ring. A PTFE vessel (5-cm diameter) was used for the measurements, and the samples were equilibrated for 2 h. The surface tension was then measured until a constant value was recorded for > 20 min.

2.5 Surface elasticity measurements

The surface elasticity data of $sPSO_2$-220/C_{14}TAB mixtures in Fig. 1 of the main text are reproduced from ref. [7]. Values of the surface elasticity were measured using a PAT1 instrument (Sinterface Technologies, Berlin, Germany). A pendant drop of the mixture was created by the device at the tip of a capillary. The capillary was situated in a closed cuvette that had a small reservoir of sample solution to limit evaporation. Each drop was equilibrated for 2 h before the start of each measurement. Harmonic oscillations of the drop surface were induced by computer. The surface area A and γ were calculated as a function of time using drop-shape analysis. The drop oscillation frequency was 0.1 Hz. At a given value of A, variation the change in γ is a measure of the dilatational surface elasticity ε. Values of ε were calculated from the amplitude ratio of the oscillating γ and A values, whereas the phase shift between the two quantities determines the dilatational surface viscosity [8].

2.6 Thin film pressure balance measurements

The maximum disjoining pressure data of $sPSO_2$-220/C_{14}TAB mixtures in Fig. 1 of the main text are reproduced from ref. [7]. Disjoining pressure isotherms were measured using porous plates with a thin film pressure balance [9]. Free-standing horizontal liquid foam films have been investigated using this method for more than 50 years [10]. Information about interaction forces, thicknesses, drainage and stabilities of thin foam films can be obtained using this technique. A description of the experimental setup can be found elsewhere in the literature [11]. The foam film is formed inside a hole of 1-mm diameter, which is situated in a porous glass disk. Prior to each measurement, the film holder was immersed for at least 2 h in the sample solution to allow sample equilibration. At the start of each measurement, the film holder was pulled out and left for 2 h to allow surface equilibration. Disjoining pressure isotherms were obtained through measurements of the foam film thickness h by interferometry while varying the applied pressure [12]. The equilibrium foam film thickness was measured after the intensity of light reflected was constant for 20 min. The disjoining pressure isotherms in ref. [7] were averaged from at least 3 measurements. The maximum value of the disjoining pressure was taken as a measure of foam film stability.

2.7 Neutron reflectometry (NR)

The NR experiments were performed on the FIGARO reflectometer at the Institut Laue-Langevin (Grenoble, France) [13]. The instrument was used with a chopper pair giving neutron pulses with 7% $d\lambda/\lambda$ in the wavelength range λ = 2–30 Å. Data acquisition was carried out at incident angles of θ = 0.62° and 3.8°. Prior to each measurement all samples were equilibrated until they reached steady state. Specular neutron reflectivity profiles determine the intensity ratio of neutrons in the specular reflection to those in the incident beam with respect to the momentum transfer, Q, defined by $Q = 4\pi\sin\theta/\lambda$.

3 NR Data Evaluation

3.1 First execution: low-*Q* compositional analysis

Neutron reflectivity data were recorded in a restricted low *Q*-range < 0.05 $Å^{-1}$ in the 2 isotopic contrasts: (1) $sPSO_2$-220/$cmC_{14}TAB$/ACMW and (2) $sPSO_2$-220/$dC_{14}TAB$/ACMW, where $cmC_{14}TAB$ is contract matched $C_{14}TAB$ (4.4%w/w $dC_{14}TAB$ in $C_{14}TAB$) and ACMW is air contrast matched water (8.1%v/v D_2O in H_2O), which both have zero a scattering length density (SLD or ρ). For contrast 1, the specular reflectivity consists only of scattering from the adsorbed polyelectrolyte, while for contrast 2, the specular reflectivity is dominated by scattering from the adsorbed deuterated surfactant [14]; in the latter case, adsorbed polyelectrolyte also contributes to the reflectivity but it has a relatively low SLD and therefore the contribution is small. This approach exploits the high flux at the natural low incidence angle of the FIGARO reflectometer, which allows separation of the weak signal of interfacial hydrogenous polyelectrolyte from the background faster and more accurately than traditional methods [3].

The background was subtracted from the data for each measurement through use of the area detector, and the residual background was determined as 1.5 x 10^{-6} from a measurement of pure ACMW. The SLD of a single interfacial layer was fixed at an arbitrary value of 2 x 10^{-6} $Å^{-2}$ in contrast 1 and 4 x 10^{-6} $Å^{-2}$ in contrast 2, and the layer thickness (*d*) was fitted using layer roughness values estimated at 3.5 Å to be consistent with the presence of capillary waves for samples with a surface tension in between that of pure water and a surfactant solution of full monolayer coverage [15]. Motofit software was used [16], which involves calculations based on the interaction of neutrons with a stratified layer model on the basis of the Abeles matrix method. Examples of reflectivity profiles are shown in Fig. SI2 where the SLD depth profiles in the inset indicate the arbitrary nature of the fixed SLDs chosen for use in the model.

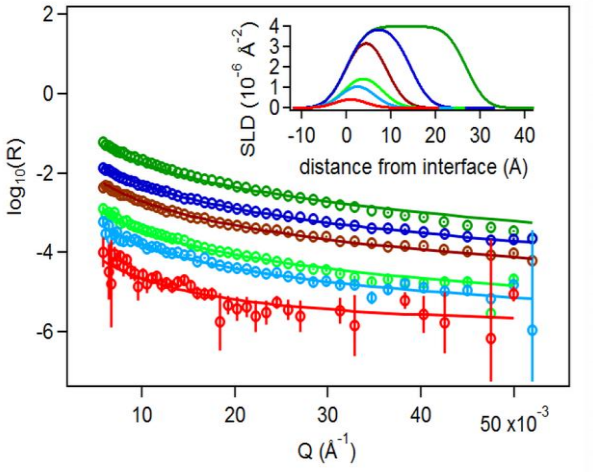

Fig. SI2. Examples of neutron reflectivity profiles and model fits recorded in a restricted *Q*-range for samples with [P] = (red) 1 × 10^{-5} (mono)M, (green) 8 × 10^{-5} (mono)M and (blue) 3 × 10^{-3} (mono)M and [S] = 10^{-4} M (light) $cmC_{14}TAB$ or (dark) $dC_{14}TAB$ in ACMW, where SLD depth profiles of corresponding colors are shown in the inset.

The low-*Q* nature of the analysis means that the results are sensitive primarily to the interfacial composition and are insensitive to the specific structure [17]. The results were used to solve the following

simultaneous equations giving the surface excesses $\Gamma_{sPSO2\text{-}220}$ and Γ_{C14TAB} for the polyelectrolyte and surfactant, respectively:

$$(\rho d)_1 = N_A(b_{sPSO2\text{-}220}\Gamma_{sPSO2\text{-}220}) \quad (1)$$

$$(\rho d)_2 = N_A(b_{sPSO2\text{-}220}\Gamma_{sPSO2\text{-}220} + b_{C14TAB}\Gamma_{C14TAB}) \quad (2)$$

where N_A is Avogadro's number, b is the scattering length of a component, Γ is its surface excess, and for a given species ρ is equal to b divided by its molecular volume. The contribution of the counterions is neglected in the data analysis, as their scattering lengths with respect to the deuterated surfactant and polyelectrolyte are just ~3% and the binding at the interface is dominated by electrostatic interactions. The values of fixed parameters b and ρ used in the model fits of this work are listed in Table SI1.

Table SI1: Values of the scattering length and SLD used in the data evaluation.

Species	b (x 10^{-5} Å)	ρ (x 10^{-6} Å^{-2})
$sPSO_2$-220	61.5	1.7
C_{14}TAB	–13.3	–0.24
cmC_{14}TAB	0	0
dC_{14}TAB	288	5.14
$C_{14}D_{29}$ Chain	286	7.16
$C_{14}H_{29}$ Chain	–15.4	–0.39
$N(CH_3)_3$Br Head Group	2.12	0.18

3.2 Second execution: full-*Q* structural analysis

Neutron reflectivity data were recorded for one bulk composition in each of the three regimes described in Fig. 1 of the main text over the full accessible *Q*-range for selected samples in 3 isotopic contrasts: (1) $sPSO_2$-220/dC_{14}TAB/ACMW, (2) $sPSO_2$-220/dC_{14}TAB/D_2O and (3) $sPSO_2$-220/C_{14}TAB/D_2O. A finite number of stratified layers of the interfacial structure were constructed, each with (1) surfactant chains, (2) surfactant head groups, (3) surfactant head groups and polyelectrolyte or (4) polyelectrolyte, with any layer except the upper layer of surfactant chains in contact with air being solvated as well.

The data in regime I were best modeled with a layer of surfactant chains of volume fraction equal to 1 in contact with the air, and a compact layer of solvated surfactant head groups and polyelectrolyte underneath. The data in regime II were most complicated to model. An equivalent structure to that in regime I was required but with two further layers. The third layer involved a bilayer of surfactant chains of low coverage and the fourth mixed outermost layer comprising surfactant head groups, additional surfactant, polyelectrolyte and solvent. The coverage of this mixed layer was also rather low. The data in regime III were modeled in a similar way to those in regime I except that there was, in addition, an extended layer of solvated polyelectrolyte that formed a third layer.

The general principles of the model respected the framework of the robust model that has been recently shown to fit well data recorded in multiple isotopic contrasts of surfactant monolayers at the air/water interface, i.e., splitting of surfactant chains and head groups into separate layers, and accounting for the presence of capillary waves with realistic layer roughness values [18]. Further, to ensure that all of the models were physically realistic, the surface excess of surfactant head groups in a given layer was made

to match faithfully that of the surfactant chains in any adjacent layers. For example, the surface excesses of surfactant chains in layer 1 *and* head groups in layer 2 of regime I are both 1.83 μmol/m^2 (taking into account both the volume fraction and the composition of layer 2). A more complex calculation was required for layer 2 of regime II where the number of head groups accounted for not only the chains in layer 1 but also those from one leaflet of the bilayer structure in layer 3. The surface excess of any component in a layer was calculated according to $\Gamma = \rho d / N_A b$.

Values of the parameters used in the model fits are listed in Table SI2. The interfacial compositions from the low-*Q* analysis (Fig. 2 of the main text) was used as a constraint in the model fits for regimes I and III, but in the case of regime II there was minimal difference to the quality of the fits with additional polyelectrolyte in the outer layer, so in this case the constraint was relaxed. The layer roughness values used were 3.5 Å (consistent with capillary waves) but the outermost diffuse layers for regime II was 4.5 Å and the extended outer layer for regime III was 20 Å.

Table SI2: Values of the parameters used in the model fits to the data shown in Fig. 3 of the main text.

LAYER	PARAMETER	REGIME I	REGIME II	REGIME III
1	Thickness (Å)	4.4	8.0	7.3
	Species	100% S-Chains	100% S-Chains	100% S-Chains
	Volume Fraction	1.00	1.00	1.00
2	Thickness (Å)	5.0	5.0	5.0
	Species	61% P + 39% S-Heads	46% P + 54% S-Heads	31% P + 69% S-Heads
	Volume Fraction	0.76	1.00	0.70
3	Thickness (Å)	N/A	22.0	80.0
	Species	N/A	100% S-Chains	100% P
	Volume Fraction	N/A	0.10	0.065
4	Thickness (Å)	N/A	15.5	N/A
	Species	N/A	15% P + 83% S + 2% S-Heads	N/A
	Volume Fraction	N/A	0.10–0.40*	N/A

* the volume fraction of layer 4 for the data corresponding to regime II was reproducible across different experiments: 0.40 for the contrasts $sPSO_2$-220/dC_{14}TAB/ACMW and $sPSO_2$-220/dC_{14}TAB/D_2O, and 0.10 for the contrast $sPSO_2$-220/C_{14}TAB/D_2O with the difference attributed to isotope-specific effects.

References

[1] Varga, I.; Campbell, R. A. *Langmuir* **2017**, *33*, 5915.

[2] Campbell, R. A.; Yanez Arteta, M.; Angus-Smyth, A.; Nylander, T.; Noskov, B.; Varga, I. *Langmuir* **2014**, *30*, 8664–8674.

[3] Campbell, R. A.; Tummino, A.; Noskov, B.; Varga, I. *Soft Matter* **2016**, *12*, 5304.

[4] Mészáros, R.; Thompson, L.; Bos, M.; Varga, I.; Gilányi, T. *Langmuir* **2003**, *19*, 609–615.

[5] Tonigold, K.; Varga, I.; Nylander, T.; Campbell, R. A. *Langmuir*, **2009**, *25*, 4036–4046.

[6] Schuster, M.; de Araujo, C. C.; Atanasov, V.; Andersen, H. T.; Kreuer, K.-D.; Maier, J. *Macromolecules* **2009**, *42*, 3129.

[7] Uhlig, M.; Miller, R.; von Klitzing, R. *Phys. Chem. Chem. Phys.* **2016**, *18*, 18414.

[8] Loglio, G.; Pandolfini, P.; Miller, R.; Ravera, F.; Ferrari, M.; Liggieri, L. Novel Methods to Study Interfacial Layers. Elsevier, Amsterdam, 2001.

[9] Exerowa, D.; Kruglyakov, M. Foam and Foam Films - Theory, Experiment, Application. Elsevier, Amsterdam, 1998.

[10] Mysels, K. J.; Jones, M. N. *Discuss. Faraday Soc.* **1966**, *42*, 42.

[11] Stubenrauch, C.; von Klitzing, R. *J. Phys.: Condens. Matter* **2003**, *1197*, R1197.

[12] Sheludko, A. *Adv. Colloid Interface Sci.* **1967**, *1*, 391.

[13] Campbell, R. A.; Wacklin, H. P.; Sutton, I.; Cubitt, R.; Fragneto, G. *Eur. Phys. J. Plus* **2011***, 126*, 107.

[14] Braun, L.; Uhlig, M.; von Klitzing, R.; Campbell, R. A. *Adv. Colloid Interface Sci.* **2017**, *247*, 130.

[15] Tikhonov, A. M.; Mitrinovic, D. M.; Li, M.; Huang, Z.; Schlossman, M. L. *J. Phys. Chem. B* **2000**, *104*, 6336.

[16] Nelson, A*. J. Appl. Crystallogr.* **2006**, *39*, 273.

[17] Angus-Smyth, A.; Campbell, R. A.; Bain, C. D. *Langmuir* **2012**, *28*, 12479.

[18] Campbell, R. A.; Saaka, Y.; Shao, Y.; Gerelli, Y.; Cubitt, R.; Nazaruk, E.; Matyszewska, D.; Lawrence, M. J. *J. Colloid Interface Sci.* **2018**, *531*, 98.